An ultra-thin organic insulator for metal-insulator-metal diodes

D. Etor, L. E. Dodd, D. Wood and C. Balocco, *member IEEE*

***Abstract*— The design and fabrication metal-insulator-metal (MIM) diodes using an ultra-thin organic insulator is presented. The insulating layer was found to be compact, highly conformal, and uniform, effectively overcoming the main design challenge in MIM diodes. The diodes have strong non-linear current-voltage characteristics with a typical zero-bias curvature coefficient 5.4 V^{-1} and a voltage responsivity of 1.9 kV/W at a frequency of 1 GHz. The fabrication of the diodes only requires low-temperature processing, is cost effective, and can potentially be ported to large-area roll-to-roll manufacturing.**

***Index Terms*—Metal-insulator-metal diodes, microwave diode, molecular electronics, octadecyltrichlorosilane.**

I. Introduction

Metal-insulator-metal (MIM) diodes have attracted much attention in recent years because of the possibility of operating at very high frequencies, well into the terahertz range, a promise first highlighted over thirty years ago [1], [2]. The MIM diode is a quantum device wherein a thin dielectric is sandwiched between two metal electrodes with dissimilar work functions, which cause an asymmetric electric current to flow through the dielectric with respect to the polarity of the electrodes. The asymmetry at zero bias can be further increased by maximizing the work function difference between the two electrodes [3]. This increases the possibility for the diode to operate without the need for an externally applied bias, making it a useful component in a wide range of applications, including radio-frequency identification (RFID) tags, thermal-energy harvesting, and high frequency detectors and mixers [4]–[6].

The fabrication of MIM diodes has been reported in the literature using several fabrication techniques [7]–[10]. In this work, the device has been fabricated using a low-cost technique where the dielectric layer consists of octadecyltrichlorosilane (OTS), an amphiphilic molecule consisting of an alkyl chain and a polar head group, commonly used to functionalize the surface of silicon dioxide (SiO_2). Its thickness is essentially determined by the length of the alkyl chain, rather than process conditions, with typical value of approximately 2 nm [11], [12]. An OTS layer was sandwiched between titanium and platinum, which have a work function difference of 1.4 eV thereby resulting in a strong non-linear current-voltage *(J-V)* characteristic.

D. Etor is with the School of Electrical and Electronic Engineering, Durham University, South Road, Durham, DH1 3LE United Kingdom (e-mail: david.etor@durham.ac.uk).

L. E. Dodd is with the School of Electrical and Electronic Engineering, Durham University, South Road, Durham, DH1 3LE United Kingdom (e-mail: l.e.dodd@durham.ac.uk).

D. Wood is with the School of Electrical and Electronic Engineering, Durham University, South Road, Durham, DH1 3LE United Kingdom (e-mail: david.wood@durham.ac.uk).

C. Balocco is with the School of Electrical and Electronic Engineering, Durham University, South Road, Durham, DH1 3LE United Kingdom (e-mail: claudio.balocco@durham.ac.uk).

II. Fabrication

A. OTS solution preparation and deposition

An OTS/hexane solution (1 part of OTS in 2000 part of hexane by volume) was prepared in a beaker and sonicated for 25 minutes to aid uniformity. A layer of titanium with a nominal thickness of 25 nm, deposited onto a borosilicate glass substrate by e-beam evaporation, was immersed in the OTS/hexane solution and left for an hour without stirring, after which it was removed and immediately dipped in hexane and sonicated for a further 15 minutes in order to remove any unwanted polymerized OTS particles that may have adhered to the titanium surface. The substrate was then baked for 30 minutes at 90 °C to complete the OTS polymerization and to remove any residual solvent.

As it can be seen in Fig. 1(a) prior to OTS deposition, the surface of the titanium film as deposited is hydrophilic, indicating the presence of OH groups, with a contact angle θ = 10°. After OTS deposition, a film is formed on the titanium surface, making it highly hydrophobic with a contact angle θ = 105°, as shown in Fig. 1(b), which is typical for an OTS covered surface [11], [13]. Atomic-force microscopy (AFM), showed no significant difference in the surface roughness of the titanium surface before and after OTS deposition. This is to be expected due to the nanometer scale thickness of the OTS SAM. Control samples fabricated without the OTS layers resulted in short circuits, confirming the insulating properties of OTS.

B. Ti/OTS/Pt diode process

Fig. 2 (not drawn to scale) shows the basic fabrication process. A bilayer of approximately 25 nm of titanium coated with 100 nm of gold was deposited by e-beam evaporation and lift-off (a). After a further photolithographic step, gold was removed by an iodine/iodide wet etching, leaving small regions of titanium exposed (b-c). After removing the

photoresist (d) the exposed titanium was coated with OTS (e) using techniques as described above. After a further photolithographic step, a thin layer of platinum with a nominal thickness of 40 nm was evaporated on the sample and lifted-off in the unexposed regions, resulting in the definition of small Ti/OTS/Pt junctions (g-h). Other metals, Ti, Ni, and Cr, where also tested for the top electrode, to confirm the dependence on the metal work-function difference. As expected Ti/OTS/Ti structures resulted in symmetric *J-V* characteristic, while Ti/OTS/Pt structures, with the highest workfunction difference, provided the highest curvature coefficient. The addition of leads and bonding pads concludes the MIM diode fabrication. A sketch of the device cross-section and a scanning electron microscopy (SEM) image of a fabricated device can be seen in the inset of Fig. 3, where the OTS layer is sandwiched between the two metal layers at the crossover of two arms which defines the MIM junction. The nominal feature size of the fabricated diode junction is 2 μm×2 μm. This process can also be used in the fabrication of MIM diodes on a flexible plastic substrate [14] since only low-temperatures are required.

III. Electrical Measurements

A. DC measurement

The diodes were electrically characterized under quasi-static conditions using a parameter analyzer. The voltage range was kept within ±0.2 V in order to avoid damaging the diode junctions, as they were found to have an irreversible breakdown voltage of ±0.35 V, which is likely due to the formation of conductive paths with defects present in the OTS film. Nevertheless, this value is comparable to other MIM structures which use a metal oxide as insulating layer [3]. A typical *J-V* characteristic is plotted in Fig. 3, showing a strong non-linearity at zero bias (i.e. $V = 0$ V). The zero-bias curvature coefficient (γ_{ZB}), defined as:

$$\gamma_{ZB} = \frac{d^2I}{dV^2} \Big/ \frac{dI}{dV}\Big|_{V=0} \tag{1}$$

was consistently found to be approximately 5.4 V^{-1}. While this value is relatively small compared to traditional GaAs Schottky rectifiers it is a highly competitive value when compared with those available in the MIM diodes literature [15].

B. High frequency AC measurement

Characterization at high frequencies (HF), from 1 MHz to 3 GHz, was carried out on the diodes using a vector network analyzer (VNA). The rectified output voltage was measured for HF powers in the range -47 to -37 dBm. To enable HF testing, ten diodes were embedded within a coplanar waveguides with a characteristic impedance of 50 Ω, matched to the characteristic impedance of the probes, thus minimizing unwanted reflections from the layout as well as reducing radiation losses.

Fig. 4(a) shows the typical rectified output voltage of the diode as a function of the HF power injected into the coplanar waveguide at a frequency of 1 GHz. while Fig. 4(b) shows how the voltage rectified by the diode changes as a function of the operating frequency with a constant input HF power of approximately 100 nW (-40 dBm). All measurements were carried at room temperature, and the input HF power compensated at different frequencies to account for the measured losses in the cables, probes and coplanar waveguides. The diode voltage responsivity R_V is defined as [17]:

$$R_V = \frac{V_{OUT}}{P_{HF}} = \left(\frac{d^2V}{dI^2} \Big/ \frac{dV}{dI}\right), \tag{2}$$

where V_{OUT} is the dc voltage rectified by the diode and P_{HF} is HF power injected by the VNA into the coplanar waveguide. Its value was determined by a linear fitting of the rectified output voltage as a function of the input HF power, shown in Fig. 4(a), and had an absolute value of approximately 1.9 kV/W at a frequency of 1 GHz, comparable to state-of-the-art Schottky-diode detectors [18].

The frequency response of the diode, measured up to 3 GHz, is shown in Fig. 4(b); it exhibits typical first-order dependence for frequencies, which can be fit by [16]:

$$|V_{DO}| = \left|\frac{V_0}{1+(f/f_C)^2}\right| \tag{3}$$

where V_{DO} is the magnitude of the voltage rectified by the diode, V_0 is the amplitude of the HF input voltage, f the frequency, and f_C the -3dB cut-off frequency typical of a first-order system. As the zero-bias resistance of the diode is much larger than 50 Ω source resistance it can be neglected in Eq. (3).

In order to determine which parameters influence the diode response, we assumed that the diode embedded in the coplanar waveguide could be described by the simple detection circuit shown in Fig. 5(a). The values of the components, capacitors and resistors, were determined by measuring the reflection coefficient of the whole structure, s_{11}, as a function of the frequency using the VNA, and converting it to the input impedance Z_{IN} using [19]:

$$Z_{IN} = Z_0\left(\frac{1+s_{11}}{1-s_{11}}\right) \tag{4}$$

where $Z_0 = 50$ Ω is the characteristic impedance of the microwave probes and VNA ports. The real and imaginary parts of Z_{IN} as a function of the frequency are plotted in Fig. 5(b). The numerical fitting of both curves, for frequencies above 0.5 GHz, resulted in a series resistance $R_S = 32$ Ω and a parallel capacitance $C_P = 3.1$ pF. The series resistance R_S is a result of the thin metal layer used for the coplanar waveguide (approximately 200 nm of gold) and of the platinum and titanium diode terminals. The parallel capacitance was much higher than expected from the parallel-plate capacitors associated to the diode junction, and it is ascribed to fringe effect of the diode leads. This was confirmed by performing electromagnetic simulations of the whole structure (using Agilent Advance Design System) in the frequency range

100 MHz-3 GHz, which is in agreement with the measured data. The resistance of the ten MIM junctions (typically of the order of tens of kΩ) was accounted for by adding lumped resistors in the simulations in order to correctly fit the lower frequency region. A comparison between the simulated input impedance and Z_{IN} is shown in Fig. 5(b). Also the accuracy of the simulated impedance suffered from some uncertainty in the OTS dielectric constant ε_r; a value of $\varepsilon_r = 3$ was assumed throughout the investigations [20].

No attempt was made in this work to match impedance the diode to the source, to avoid the introduction of further unknowns in the experimental setup. Both narrow- and wide-band matching network are however being developed to improve the responsivity and power conversion at specific frequency bands. More complex models are also under investigation to fully describe the diodes at much higher frequencies. The emphasis is both on diodes embedded into a coplanar waveguides, which is a suitable structure for testing up to sub-terahertz frequencies, as well as diodes coupled to microantennas for testing with a terahertz VNA in free space.

IV. Conclusion

A low-cost MIM diodes with an OTS layer as an ultra-thin insulator have been produced successfully. Quasi-static and high-frequency analysis showed that the diodes have strong non-linear *J-V* characteristics with a typical zero-bias curvature coefficient of approximately 5.4 V^{-1} and voltage responsivity of 1.9 kV/W at a frequency of 1 GHz. The process developed for fabricating these diodes is very cost effective, and can be readily employed in the roll-to-roll commercial production of MIM diodes on flexible substrates. Further work is ongoing to investigate the device reliability, and to reduce the feature size to sub-100 nm dimensions in order to increase the cut-off frequency into the terahertz range.

Acknowledgment

David Etor wishes to thank the Petroleum Technology Development Fund (PTDF) of Nigeria for the award of a PhD scholarship.

References

[1] R. E. Drullinger, K. M. Evenson, D. A. Jennings, F. R. Petersen, J. C. Bergquist, L. Burkins, and H.U. Daniel. (1983, Jan.). 2.5 THz Frequency Difference Measurements in the Visible Using Metal-Insulator-Metal Diodes. *Appl. Phys. Lett.* [Online]. *42(2),* pp. 137–138. Available: http://tf.boulder.nist.gov/general/pdf/536.pdf

[2] K. J. Siemsen and H. D. Riccius. (1984, Jun.). Experiments With Point-Contact Diodes in the 30-130 THz Region. *Appl. Phys. A.* [Online]. *35(3),* pp. 177–187. Available: http://link.springer.com/article/10.1007%2FBF00616972

[3] L. E. Dodd, A. J. Gallant, and D. Wood. (2011, Oct.). Optimizing MOM Diode Performance via the Oxidation Technique. Presented at IEEE Conf. Sens, [Online]. pp. 176–179. Available: http://ieeexplore.ieee.org/xpls/abs_all.jsp?arnumber=6127347&tag=1

[4] S. Jinpeng, W. Xin'an, L. Shan, Z. Hongqiang, H. Jinfeng, Y. Xin, F. Xiaoxing, and G. Binjie. (2012, Nov.). Design and Implementation of an Ultra-Low Power Passive UHF RFID Tag. *J. Semicond.* [Online]. *33(11).* pp. 115011-1–115011-5. Available: http://www.jos.ac.cn/bdtxbcn/ch/reader/create_pdf.aspx?file_no=12041203

[5] Y. Pan, C. V. Powell, A. M. Song, and C. Balocco. (2014, Dec.). Micro Rectennas: Brownian Ratchets for Thermal-Energy Harvesting. *Appl. Phys. Lett.* [Online]. *105(25).* pp. 253901-1–253901-4. Available: http://scitation.aip.org/content/aip/journal/apl/105/25/10.1063/1.4905089

[6] P. Periasamy, J. J. Berry, A. A. Dameron, J. D. Bergeson, D. S. Ginley, R. P. O'Hayre, and P. A. Parilla. (2011, May). Fabrication and Characterization of MIM Diodes Based on Nb/Nb2O5 via a Rapid Screening Technique. *Adv.Mater.* [Online]. *23(27).* pp. 3080–3084. Available: http://onlinelibrary.wiley.com/doi/10.1002/adma.201101115/abstract

[7] L. E. Dodd, A. J. Gallant, and D. Wood. (2012). Ti-TiOx-Pt Metal-Oxide-Metal Diodes Fabricated via a Simple Oxidation Technique. Presented at MRS proc. [Online]. pp. 1–4, Available: http://journals.cambridge.org/action/displayAbstract?fromPage=online&aid=8476108&fileId=S1946427412000723

[8] L. E. Dodd, A. J. Gallant, and D. Wood. (2013, Aug.). Controlled Reactive ion Etching and Plasma Regrowth of Titanium Oxides of Known Thickness for Production of Metal-Oxide-Metal Diodes. *IET Micro and Nano Lett.* [Online]. *8(8).* pp. 476–478. Available: http://www.crossref.org/iPage?doi=10.1049%2Fmnl.2013.0177

[9] L.E. Dodd, M.C. Rosamond, A.J. Gallant and D. Wood. (2014, Jul.). Development of Phase Shift Lithography for the Production of Metal-Oxide-Metal Diodes. *IET Micro and Nano Lett.* [Online]. *9(7).* pp. 437–440. Available: http://www.crossref.org/iPage?doi=10.1049%2Fmnl.2014.0102

[10] L.E. Dodd, S.A. Shenton, A.J. Gallant and D. Wood. (2015, May). Improving Metal-Oxide-Metal (MOM) Diode Performance via the Optimization of the Oxide Layer. *J. Electron. Mater.* [Online]. *44(5).* pp.1361–1366. Available: http://link.springer.com/article/10.1007%2Fs11664-015-3624-9

[11] M. H. Jung and H. S. Choi. (2009, Nov.). Characterization of Octadecyltrichlorosilane Self-Assembled Monolayers on Silicon (100) Surface. *Korean J. Chem. Eng*. [Online]. *26(6),* pp. 1778–1784. Available: http://link.springer.com/article/10.1007%2Fs11814-009-0249-9

[12] S. Kim, H. Sohn, J. H. Boo and J Lee. (2008, Jan.). Significantly Improved Stability of N-Octadecyltrichlorosilane Self-Assembled Monolayer by Plasma Pretreatment on Mica", *Thin Solid Films.* [Online]. *515(6).* pp. 940–947. Available:

http://www.sciencedirect.com/science/article/pii/S0040609007008723

[13] J. Dong, A. Wang, K.Y. S. Ng, and G. Mao. (2006, Dec.). Self-Assembly of Octadecyltrichlorosilane Monolayers on Silicon-Based Substrates by Chemical Vapor Deposition. *Thin Solid Films* [Online]. *515(4).* pp. 2116–2122. Available: http://www.sciencedirect.com/science/article/pii/S0040609006008418

[14] A. Kaur, X. Yang, and P. Chahal. (2014, May). Study of Microwave Circuits Based on Metal-Insulator-Metal (MIM) Diodes on Flex Substrates. Presented at Electron. Compon. Technol. Conf . [Online]. pp. 2168–2174. Available: http://ieeexplore.ieee.org/xpls/icp.jsp?arnumber=6897603

[15] B. Tiwari, J. A. Bean, G. Szakmany, G. H. Bernstein, P. Fay and W. Porod. (2009, Aug.). Controlled Etching and Regrowth of Tunnel Oxide for Antenna-Coupled Metal-Oxide-Metal Diodes. *J. Vac. Sci. Technol*. [Online]. *27(5).* pp 2153–2160. Available: http://scitation.aip.org/content/avs/journal/jvstb/27/5/10.1116/1.3204979

[16] A. M. Cowley, and H. O. Sorensen. (1966, Dec.). Quantitative Comparison of Solid State Microwave Detectors. *IEEE Trans. Microwave Theory Tech.* [Online]. *14(12).* pp. 591-592. Available: http://ieeexplore.ieee.org/xpls/abs_all.jsp?arnumber=1126337&tag=1

[17] J. L. Hesler and T. W. Crowe. (2007, Mar.). Responsivity and Noise Measurements of Zero-Bias Schottky Diode Detectors. Presented at the 18th Int. Symp. on Space Terahertz Technol. [Online]. pp. 89-92. Available: http://ww.w.vadiodes.com/VDI/pdf/VDI%20Detector%20Char%20ISSTT2007.pdf

[18] J. L. Hesler and T. W. Crowe. (2007, Sept.). NEP and Responsivity of THz Zero-Bias Schottky Diode Detectors. Presented at the Jt. Int. Conf. Infrared Millimeter Waves 14th Int. Conf. Terahertz Electron. [Online]. pp. 844 – 845. Available: http://ieeexplore.ieee.org/xpls/abs_all.jsp?arnumber=4516758

[19] D. M. Pozar, "Oscillators and mixers" in *Microwave Engineering*, 4th ed., Wiley, New York: 2011, pp. 617-622.

[20] D. Vuillaume, P. Fontaine, J. Collet, D. Deresmes, M. Garet, and F. Rondelez. (1993, Aug.). Alkyl-Trichlorosilane Monolayer as Ultra-Thin Insulating Film for Silicon MIS Devices. *Microelectron. Eng.* [Online]. *22(1–4)* pp. 101-104. Available: http://www.sciencedirect.com/science/article/pii/016793179390140Z

David Etor was born in Kaduna Nigeria in 1983. He received an HND degree in electrical engineering (power and machines) from Kaduna Polytechnic, Kaduna Nigeria in 2008, and an MSc in electrical power from Newcastle University, Newcastle Upon Tyne, UK in 2012. He is currently pursuing a PhD degree in microsystems technology at Durham University, Durham, UK.

His current research interest includes planar antennas and ultra-high speed metal-insulator-metal (MIM) diodes for the collection and rectification of electromagnetic radiation.

Mr. David Etor is a student member of The Institute of Engineering and Technology (IET).

Linzi E. Dodd was born in Newcastle upon Tyne, UK in 1987. She received a first class MEng (hons) degree in Electronic Engineering from Durham University, UK in 2009, and a PhD in microsystems technology from the same institution in 2014.

She is currently employed as a Research Associate as part of the Microsystems Technology group in the School of Engineering and Computing Sciences in Durham University. Her research interests include MOM diodes, reducing friction in fluid flow in pipes, and development of a single cell thermo-electrically actuated microgripper.

David Wood received a BSc (hons.) degree in Physics in 1979, and a PhD in Physics in 1984, from the University of Hull.

From 1984 to 1987, he was a Senior Research Engineer at STC Technology Ltd. In Harlow, Essex, working on fabrication techniques for the manufacture of gallium arsenide ICs, and quaternary laser diodes and photodetectors. Since 1989, he has been at Durham University, and received a promotion to a personal chair in 2005.

He is the author of one book, three patents and more than 170 journal and conference contributed papers. He leads the Electronics Research Group at Durham University, where his own research interests are in MIM diodes and their applications, microscale surface texturing for hydrophobic behavior and the development of a single cell microgripper.

Claudio Balocco was born in Milan, Italy, where he received his MSc in Electronic Engineering from the Politecnico di Milano. He then moved to the University of Manchester, United Kingdom, to complete his PhD in semiconductor nanodevices. He is a Lecturer in Electronics in the School of

Engineering and Computing Sciences at Durham University, following appointments as a Research Associate at the University of Manchester. His research interests include the design of novel nanodevice architectures and circuits in organic and metal-oxide thin films, ultra-fast nanodevices for THz applications and large-area micro- and nano-fabrication techniques, as well as transport phenomena in self-assembled quantum dots. More recently, his interest focuses on the interaction of thermal radiation with semiconductor nanodevices with applications envisaged in THz imaging and energy harvesting.

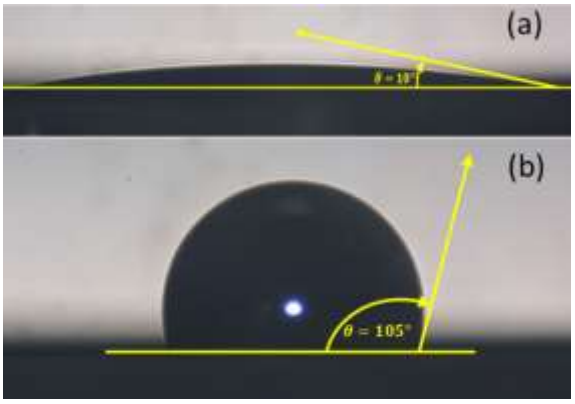

Fig. 1. Contact angle of titanium (a) before, and (b) after OTS deposition, showing increased hydrophobicity.

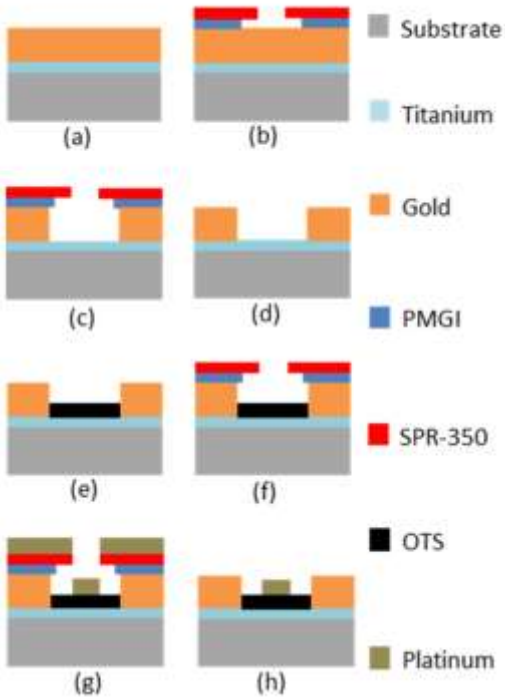

Fig. 2. The Ti/OTS/Pt MIM diode fabrication process. (a) Ti/Au bilayer on borosilicate glass. Photolithographic patterning (b) followed by Au wet etching (c). Photoresist stripping (d) and OTS deposition (e). Photolithographic patterning (f), Pt deposition (g) and lift-off (h).

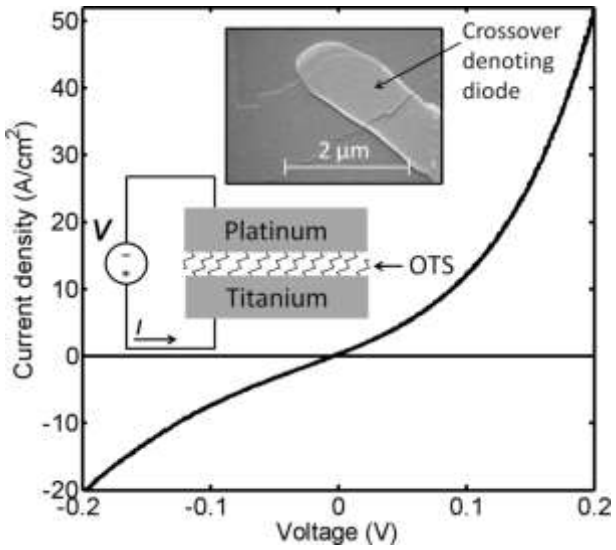

Fig. 3. Typical *J-V* characteristics of a Ti/OTS/Pt MIM diode. The insets show a sketch of the diode cross-section and a SEM image of a fabricated diode. The titanium and platinum layers act as the anode and the cathode, respectively.

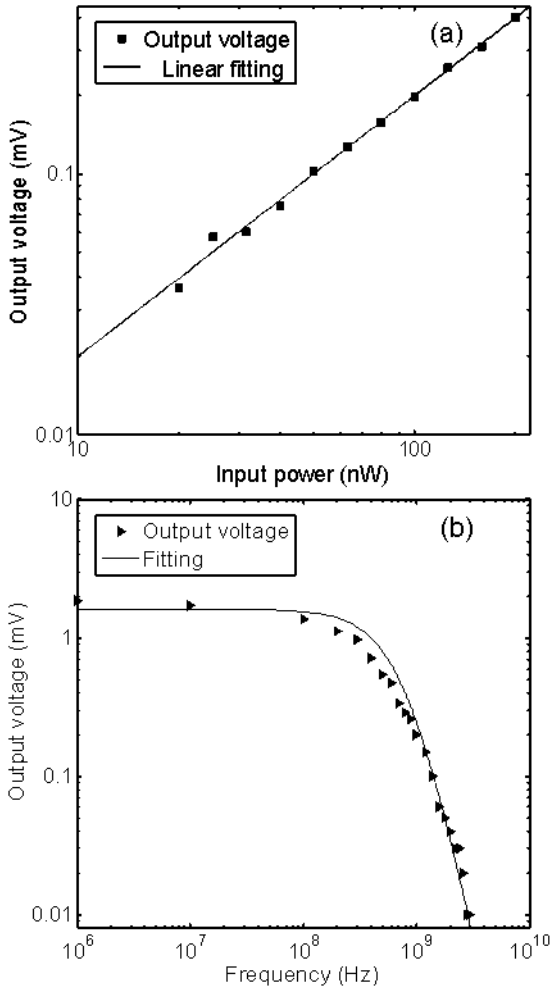

Fig. 4. (a) Rectified voltage as a function of input HF power at a frequency of 1 GHz. (b) Rectified voltage as a function of the frequency. The input power was kept constant at approximately 100 nW (-40 dBm). Cable and probe losses were compensated to maintain a constant power at the diode terminals.

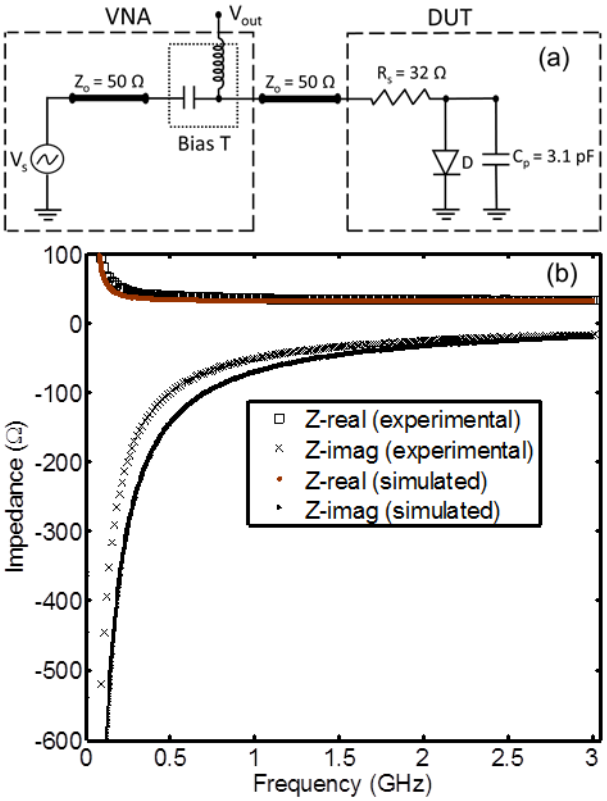

Fig. 5. (a) Equivalent high-frequency circuit diagram for the diode characterization. The series resistance R_S and parallel capacitance C_P where extracted by measuring and fitting the reflection coefficient s_{11} as a function of the frequency. (b) Measured and simulated diode impedance as a function of the frequency.